DISCRETE-VORTEX SIMULATION OF PULSATING FLOW ON A TURBULENT LEADING-EDGE SEPARATION BUBBLE

13-15 JANUARY 1992

Hyung Jin Sung and Jae Wook Rhim
Department of Mechanical Engineering, Korea Advanced Institute of Science and Technology, Taejon, KOREA
and
Masaru Kiya
Department of Mechanical Engineering, Hokkaido University, Sapporo, JAPAN

Abstract

Studies are made of the turbulent separation bubble in a two-dimensional semi-infinite blunt plate aligned to a uniform free stream when the oncoming free stream contains a pulsating component. The discrete-vortex method is applied to simulate this flow situations because this approach is effective to represent the unsteady motions of turbulent shear layer and the effect of viscosity near the solid surface. The numerical simulation has fairly reasonable predictions with the experimental results which have already performed. A particular frequency given a minimum reattachment which is related to the drag reduction and the most effective frequency is dependent on the most amplified shedding frequency. The turbulent flow structure is scrutinized, which includes the time-mean and fluctuations of the velocity and the surface pressure, together with correlations between the fluctuating components. A comparison between the pulsating flow and the non-pulsating flow at the particular frequency of the minimum reattachment length of the separation bubble suggests that the large-scale vortical structure is associated with the shedding frequency and the flow instabilities.

Introduction

An improved understanding of pulsating flow characteristics on the turbulent separation bubble is useful in the design of aerodynamic high-speed vehicles and of pulsating turbomachineries. In this study, the separation bubble is generated by flow separation from a sharp leading-edge of a blunt circular cylinder whose axis is aligned parellel to the approaching main flow. Relevant experimental studies have been carried out by Kiya et al.[1] with a view toward the control of a turbulent leading-edge separation bubble.

Control of the separation bubbles by sinusoidal perturbations has been reported by many researchers[2,3]. Roos and Kegelman[2] obtained the reattachment length in a backward-facing step flow as a function of the level and frequency of the perturbation. Sigurdson and Roshko[3] analyzed the structure and control of a turbulent reattaching flow; the reduction of the pressure drag, bubble height and reattachment length were found to depend critically on the forcing frequency.

In order to numerically simulate pulsating flow on a turbulent leading-edge separation bubble, the discrete-vortex model is applied. This approach has been demonstrated to be effective in representing the unsteady motions of turbulent separation bubble[4]. The finite-difference simulation of the averaged Navier-Stokes equation with turbulence models has the advantage in computational accuracy and applicability. However, it is currently limited to the ranges of low Reynolds numbers for separated unsteady flows.

The discrete-vortex model is known to be a powerful tool for simulating unsteady separated flows of high Reynolds numbers[4,5]. The separating flow at the leading edge is represented by a combination of an inviscid potential flow and discrete vorticies. The effect of viscosity near the solid surface is incorporated in the model. The reduction in the circulation of elemental vortices is also introduced as a function of their ages in order to represent the three-dimensional deformation of vortex filaments. Details regarding the numerical procedures can be found in Ref. 5. The ability of the discrete vortices to adequately represent pulsating

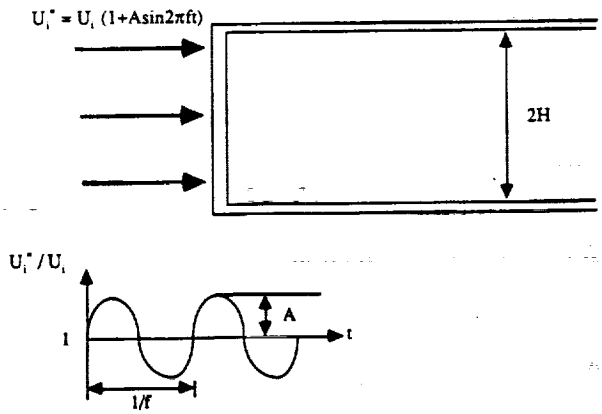

(a) Pulsating flow

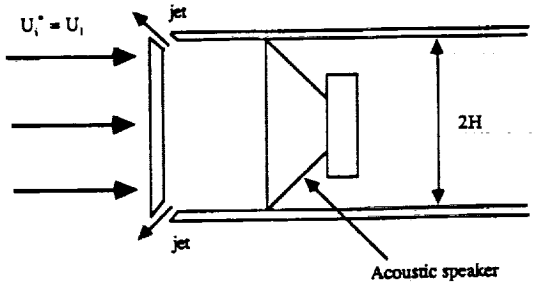

(b) Experimental apparatus with acoustic speaker

Fig. 1 Experimental apparatus and numerical analogy

continuous vortex sheetes in the separating bubbles has been tested in Ref. 6-7.

In this paper, we consider the specific example of the flow past a two-dimensional flat plate with finite thickness and a blunt leading-edge, which is aligned parallel to a uniform approaching stream. The pulsation was provided by a sinusoidally oscillating jet issued from a thin slit along the separation edge. Therefore, in the numerical simulation, the oncoming free stream was assumed to contain a sinusoidally-varying pulsating component. The entire flow field in the separation bubble is affected mainly by the dynamics near the leading-edge where separation occurs (Fig. 1).

The purpose of this study is to examine the details of the turbulent leading-edge separation bubble by discrete-vortex model. The two key parameters characterizing the free stream are the amplitude of pulsation A, and the frequency parameter St (=fH/U_i). The effects of the separation bubble on the forebody drag, the reattachment length and the lock-on effect between the pulsating frequency and the shedding frequency are investigated. The turbulent flow structure is also scritinized, which includes the time-mean and fluctuations of the velocity and the surface pressure, together with the correlations between the fluctuating components. The effect of pulsation on the minimum reattachment length of the separation bubble is examined in detail. This will show that the large scale vortical structure is closely linked with the issues of the shedding frequency and the flow instabilities.

Discrete-vortex model

The leading-edge separation bubble of a blunt two-dimensional body is considered. This flow geometry is basically the same as the flow configuration of Kiya[5]. Specifics regarding the utilization of discrete-vortex method can be found in their studies. The separation bubble is generated by flow separation from a sharp leading-edge of a blunt two-dimensional body. The dimension of the flat plate is of finite thickness(H) and semi-infinite length. The interactions between the two separation bubbles at the corners are assumed to be minimal. Thus, the symmetry condition is applied in this problem. The geometry of the body is given in Fig.2.

The Schwartz-Christoffel transformation is used to project the exterior region of the body (the physical plane, z-plane) into an upper half plane (the transformed λ-plane). The transformation is given by

$$z = \frac{H}{\pi}[(\lambda^2-1)^{1/2} - \cosh^{-1}\lambda] + iH \qquad (1)$$

The upstream free stream velocity U_i contains a pulsating component, therefore,

$$U_i^* = U_i(1+A\sin 2\pi ft) \qquad (2)$$

where f is the pulsating frequency and A is the amplitude of pulsation. If the flow has no pulsation, i.e., A=0, U_i^* reverts directly to the constant velocity at upstream infinity U_i. The complex potential w_r induced by the discrete vortices is given by

$$w_r = \sum_{j=1}^{N} \frac{iK_j}{2\pi} \log \frac{\lambda - \lambda_j}{\lambda - \lambda_j^*} \qquad (3)$$

where N is the total number of vortices in the flow field, and j is the position of the jth vortex in the transformed plane with its complex conjugate and K_j denotes its circulation. The complex potential w for the entire flow field is the sum of w_i and w_r by superposition, i.e., $w=w_r+w_i$, where w_i is the complex potential for the

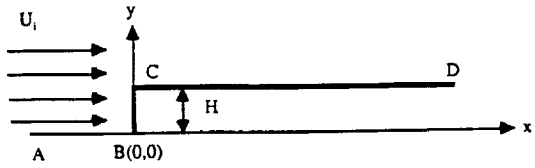

(a) Physical z plane

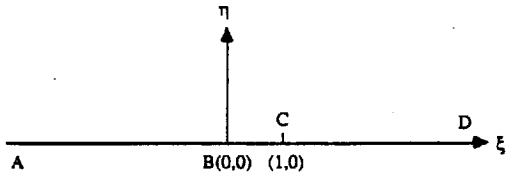

(b) Transformed λ plane

Fig. 2 Geometry of flow

irrotational flow around the body.

The velocity field in the physical plane is given by

$$u - iv = \frac{dw}{dz} = \frac{dw}{d\lambda}\frac{d\lambda}{dz} \tag{4}$$

where u and v are the velocity components in the x- and y-directions, respectively. The velocity at a vortex point, the kth vortex, has to be obtained by differentiating with Taylor expansion and the complex invariant,

$$u_k - iv_k = \frac{\frac{U_i}{\pi} + \sum_{j=1}^{N}\frac{iK_j}{2\pi(\lambda_k - \lambda_j)} - \sum_{j=1}^{N}\frac{iK_j}{2\pi(\lambda_k - \lambda_j^*)} - \frac{iK_k}{4\pi(\lambda_k^2 - 1)}}{\left(\frac{dz}{d\lambda}\right)_{\lambda=\lambda_k}} \tag{5}$$

where dw_k/dz is deduced from taking the appropriate limit as $z \to z_k$.

The convection of vortices was advanced by a second order scheme with a small time interval, the nascent vortices have to be calculated at a much smaller time interval. Since the velocity at the leading-edge should be finite, the complex potential should satisfy the Kutta condition at the edge

$$(dw/d\lambda)_{\lambda=1}=0. \tag{6}$$

The vortices are shed from the leading-edge into the separation bubble as a result of the separation. The rate of vorticity shedding was determined through the relationship, which was inferred from the experimental results[8]

$$\frac{Kn}{\Delta t_v} = \frac{1}{2}\left(\frac{dw}{dz}\right)^2_{z=i(H+\varepsilon)} \tag{7}$$

where Kn is the initial strength and the position of the nascent vortex is assumed to be $i(H+0.5\varepsilon)$, and Δt_v is the time interval between the introduction of the nascent vortices. The position of the nascent vortex is assumed to be $i(H+\varepsilon)$, where ε is an approximate initial value. The strength and location of the nascent vortices can be adjusted by an appropriate iteration scheme satisfying the Kutta condition[5].

The reduction of the circulation of every vortex is modelled by [5].

$$\frac{K(t)}{Kn} = 1 - \exp\left(-\frac{a^2 Re}{4U_i t/H}\right). \tag{8}$$

where K(t) is the circulation at time t, a is an adjustable constant, and Re denotes the Reynolds number $U_i(H/\nu)$ and ν the kinematic viscosity of the fluid. The destruction and coalescence of vortices are assumed to be proportional to the viscous core radius of each vortex. Physically, the removal of potential vortex may be regarded as corresponding to the destruction of vorticity in the shear layer by interaction with the boundary layers along the surface. The decay law (8) was deduced from the exact solution of Navier-Stokes equations for a single rectilinear viscous vortex if r is replaced by the radial distance from the center of the vortex. After carring out a number of preliminary calculation, the value of the product $a^2Re = 60$ was employed, and this was found to achieve satisfactory agreement with experimental result [5]. It may be noted that an optimum value of a^2Re depends on the particular type of flow considered.

The pressure coefficient Cp can be calculated from the Bernoulli equation,

$$C_p = \frac{P - P_i}{\frac{1}{2}\rho U_i^{*2}} = 1 - \frac{2}{U_i^{*2}}\frac{\partial\phi}{\partial t} - \frac{1}{U_i^{*2}}\left(\frac{dw}{dz}\right)^2 \tag{9}$$

where p_i is the pressure of the free stream, ρ the density of fluid and ϕ the velocity potential.

In the course of computations, some vortices approach

very closely the wall of the blunt body. Consequently, due to the presence of image vortices, these vortices would have unreasonably large velocities. In order to rectify this computational problem, vortices that approched the wall nearer than the depth of 0.02H were removed from the flow field. Since the transport of momentum and vorticity were negligible in the far field downstream, vortices and their images that were located further than the region 25H were also removed from the computation.

Since a large number of vortices exist with random locations in the flow field, it is probable that some vortices attain small separation and, therefore, produce velocity jumps at each other's positions due to the absence of viscosity. In order to alleviate this difficulty, the concept of the cut-off vortex, which was originally suggested by Chorin[9], is also employed, i.e.,

$$\psi^{o} = \frac{K \log r}{2\pi} \quad (r > \sigma)$$
$$= \frac{K(r/\sigma)}{2\pi} \quad (r \le \sigma) \qquad (10)$$

where ψ^{o} is the stream function of the vortex and σ the cut-off radius. The numerical value σ = 0.05H was adopted in this simulation . The concept of the cut-off vortices was justified in that the vortex blob in discrete-vortex simulation is basically different from that of potential flow theory, say, the point vortex.

It is noted again that the viscosity of fluid is instrumental in enforcing the no-slip flow condition. Since the discrete-vortex simulation is started from the inviscid flow, an appropriate procedure should be devised to include the viscous effect for the turbulent separation bubble and the shear layer. The viscosity of fluid gives rise to the displacement thickness in the boundary layer and, thereby, transfers momentum to the direction of transverse velocity. For this purpose, an artificial transverse velocity V_d(=0.0125U_i) was added uniformly to the edge of the shear layer.

It seems that the vortex distributions and wave forms of flow field evolve to be statistically stationary at times $U_i t/H > 80$. In this sense, the mean values and fluctuating components were calculated between the interval of $80 < U_i t/H < 280$. The non-dimensional time step t for the movement of the vortices was 0.16H / U_i and the time interval Δt, between the introduction of the nascent vortices was 0.32H / U_i (= 2Δt).

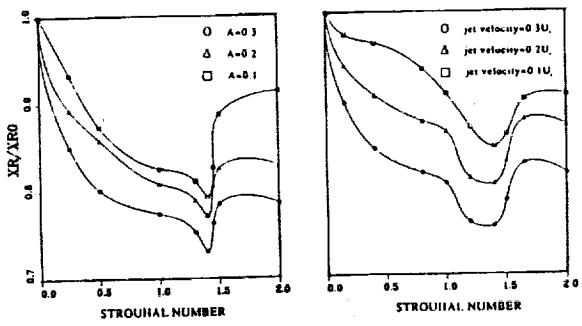

(a) Numerical result (b) Experimental result

Fig. 3 Comparison of X_r/X_{ro} between experiment and computation

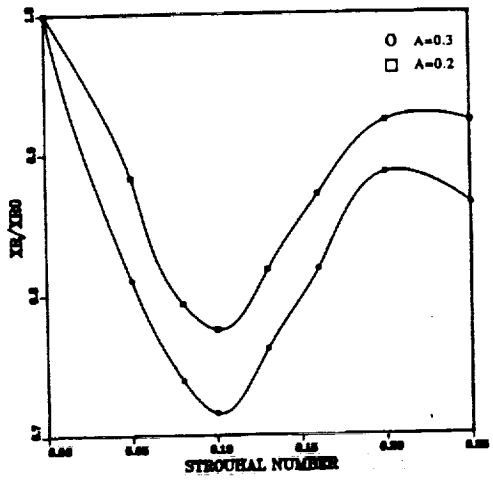

Fig. 4 Reattachment length(X_r/X_{ro}) with Strouhal number

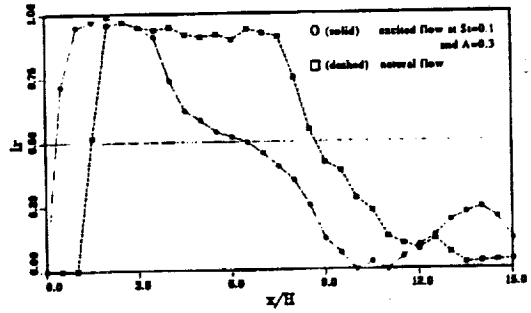

Fig. 5 Reverse flow intermittency distribution

Results and discussion

It is important to verify the aforementioned analogy between the sinusoidal oscillating jet at the separation edge and the pulsating freestream flows by the present discrete-vortex method. Toward this end, the reattachment length normalized in the form X_r/X_{ro} is plotted in Fig.3 against the non-dimensional frequency, i.e., the Strouhal number St for three different levels of the perturbation. It is noteworthy that the comparision gives a fairly consistent prediction, and this supports the assertion that this analogy seems to be reasonable. The most interesting feature of Fig.3 is that the reattachment length attains a minimum at about St=1.4 for both cases, while the amplitude affects only on the total size of reattachment. This implies that the separation bubble is affected mainly by the frequency of perturbation.

In the present study, the turbulent structures are scrutinized with the comparisons for the non-pulsating flow, natural flow(A=0) and for the perturbed flow at A=0.3 and St=0.1. It should be noted that the condition of flow pulsation was selected such that a maximum reduction of reattachment length for this two-dimensional flow configuration can be realized not for the circular blunt body (Fig. 4). For this two cases, the reverse-flow intermittency is displayed in Fig. 5. The reattachment position is defined as the point where the intermittency, I_r has the value of 0.5. In this figure, it is noticed that the reattachment position(X/H=6.5) of perturbed flow is much reduced in comparision to that of non-pulsating flow(X/H=9.1). This agrees with the experimental result[5].

Fig. 6 shows the distribution of surface velocity under the same condition. In a perturbed flow, the position of zero surface velocity is located slightly upstream of the reattachment position while the same position is maintained in natural flow. This means that the reverse flow intensity of perturbed flow is much stronger than that

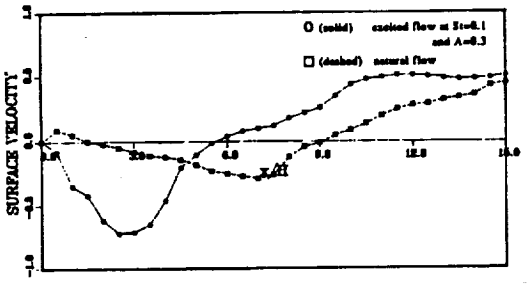

Fig. 6 Surface velocity distribution

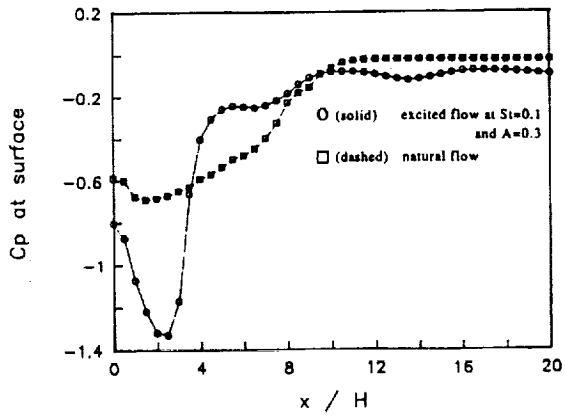

Fig. 7 (a) Time-mean pressure coefficient distribution along the surface

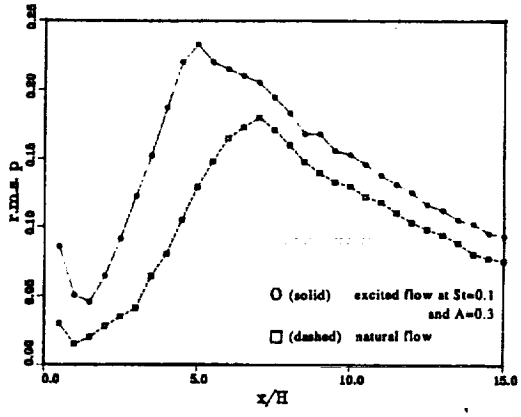

Fig. 7 (b) R.m.s. pressure distribution along the surface

of natural flow, and the feed back of fluid toward upstream of perturbed flow is active.

The distributions of pressure and its fluctuating pressure along the plate surface are shown in Fig. 7. This points to the relation with the flow reattachment for both perturbed and natural flows. It is known that the flow reattachment occurs at near the mean pressure recovery region. It is found that the mean pressure coefficient of perturbed flow at separation line is smaller than that of natural flow (Fig. 7(a)). This implies that the pressure drag is reduced when the flow is perturbed. In the pressure fluctuations of Fig.7(b), this feature of reattachment position can be elucidated more clearly. The r.m.s. of pressure fluctuation is relatively small near the separation region and then it increases along with the downstream and reaches maximum just in front of reattachment position. This region is also the same position of the maximum mean pressure recovery rate. In turbulent shear layer, it is believed that the flow has its own natural

instability and unsteadiness and the flow disturbance can be amplified most effectively at the appropriate pulsation. This is called the most effective frequency, St_{max}. This effect of amplification is maximized at the flow reattachment region, so the motion of large-scale vortices in this region are the most important elements that can decide the characteristics of the entire flow field.

In passing, it can be found in Fig. 7(a) that the pressure coefficient at separation point(C_{ps}) for the pulsating flow is reduced considerably about 30% than that of non-pulsating flow. Reduction of C_{ps} reproduces the reduction of pressure drag of the body. The maximum reduction of C_{ps} is also observed at St_{max}. This agrees well with the experimental result of Sigurdson and Roshko[3]. Koenig[10] studied the relation between C_{ps} and the drag coefficient (C_{ps}) of fluid bodies, and it gives

$$C_{ps}=0.8+0.2C_{ps}. \qquad (11)$$

From this relation, it can be noticed that the drag of the body (C_{ps}) is decreased approximately 6.25% when perturbed, i.e., $C_{ps}=0.68$ for non-pulsating flow while $C_{df}=0.64$ for pulsating flow.

The main reason of drag reduction can be explained in two ways. First, the pulsating perturbation invokes vortex coalescence in the separation bubble and then it causes the enhancement of flow spreading rate. Since the downstream flow rate is increased due to these phenomena, it gives the drag reduction. It means that the enhancement of vortex merging and flow spreading rate is strongly dependent upon the pulsating frequency. This can be analyzed as a preferred mode in Ref. 10. Next, the perturbation increases the entrainment from the outer irrotational flow. This causes the reduction of curvature of the time-mean streamlines near separation line and it deduced the large pressure gradient. Thus it decreases C_{ps} and C_{df}. It is also found that the maximum of entrainment rate is observed at St_{max}.

Many experimental results reveal that the effect of pulsation on flow structures is observed mostly at the comparatively lower frequency region[2,3,11,12]. At a particular frequency, the vortex coalescence is surprisingly enhanced. It causes that the reduction of recirculating separation bubble and flow drag of the body.

The distributions of the time-mean velocities U and V are displayed in Fig. 8. The difference between non-pulsating flow and pulsating flow is seen to be negligible near the separation line where vortices are just formed out. However, the effect of perturbation is evident in the

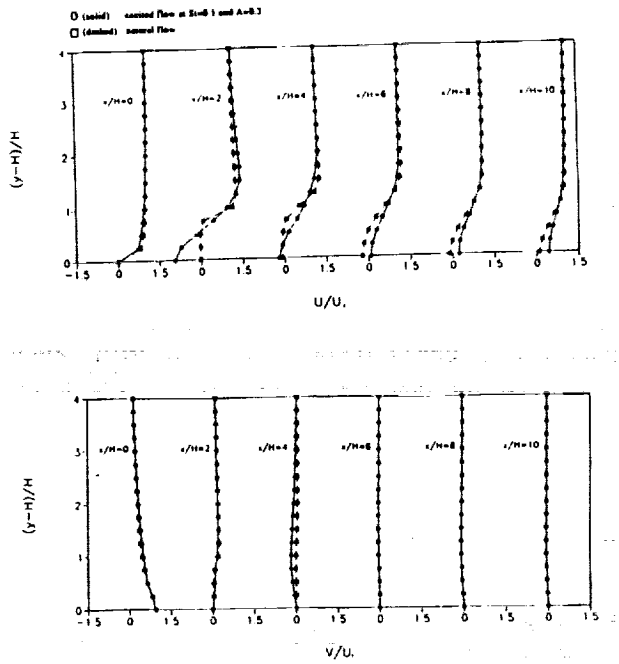

Fig. 8 Distribution of U/U_i and V/U_i along the downstream distance

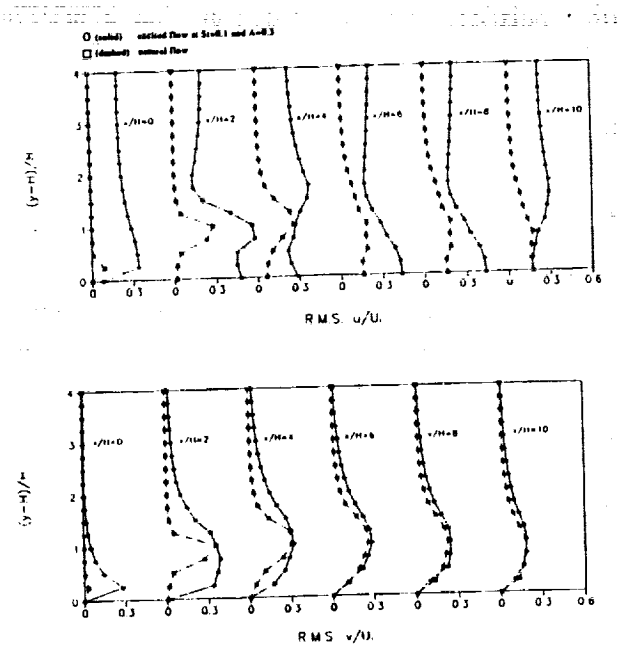

Fig. 9 Distribution of r.m.s. u/U_i and r.m.s. v/U_i along the downstream distance

reattachment region. The relatively large value of V at the separation line is due to the abrupt decrease of the curvatures of streamlines. Fig. 9 shows the r.m.s of velocity fluctuations. The turbulence level of perturbed flow is found to be considerably higher than that of natural flow.

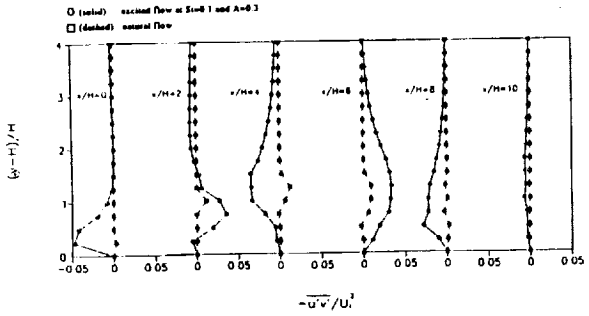

Fig. 10 Distribution of Reynolds shear stress $\overline{-u'v'}/U_i^2$

The distributions of the Reynolds stress are shown in Fig. 10. In perturbed flow, it is noteworthy that Reynolds stresses have negative values at x/H=0,4 and 8. Hussain[13], in his study on the coherent structure of turbulent shear layer, proposed that Reynolds shear stress can have negative values of vortical structure in a certain configuration where vortex coalescence process is dominant. Furthermore, since perturbation strengthens the fluctuating components in shear layer, so the mean velocity may be affected by these fluctuating velocities. The characteristic wave length of vortices can be given as follows[12];

$$\frac{L}{H}=\frac{U_c}{U_i}St^{-1} \qquad (12)$$

where U_i is the convection velocity of vortices and St_{max} is the most amplified shedding frequency, which will be referred later. Suppose the value of U_c/U_i was 0.5 [14], then L has the value of about 5H. This agrees that the locations of negative Reynolds stress are found to be nearly identical to the multiples of L. This relation reduces that negative Reynolds shear stress are brought about by the enhancement of vortex coalescence by pulsation and the positions are closely related with the characteristic wave length. From this, it can be predicted that the vortex merging is observed at every characteristic wave length in separation bubble.

The patterns discrete-vortices in the separation bubble at a certain time(t=288H/U_i) for both cases are plotted in Fig. 11. It may be noted that large-scale vortices are more evident in perturbed flow. In addition, the rolling-up behavior of large-scale vortices, the merging of vortices and the vortex-shedding from separation bubble to downstream are also observed. It is noteworthy that the concentration of discrete-vortices occurs at each multiples of L. It gives a numerical validation for negative Reynolds shear stresses in separation bubble.

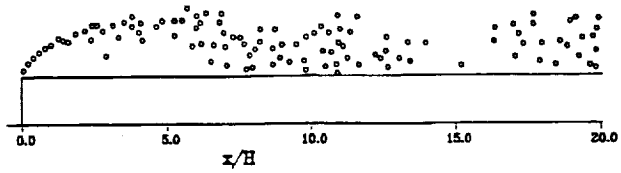

Fig. 11 (a) Distribution of discrete-vortices in unperturbed flow at t = 288 H/U_i

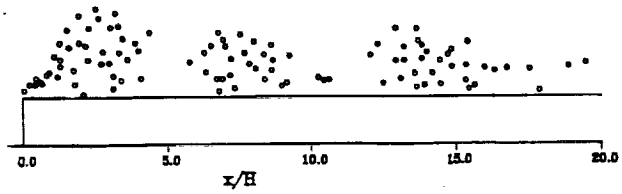

Fig. 11 (b) Distribution of discrete-vortices in perturbed flow at t = 288 H/U_i

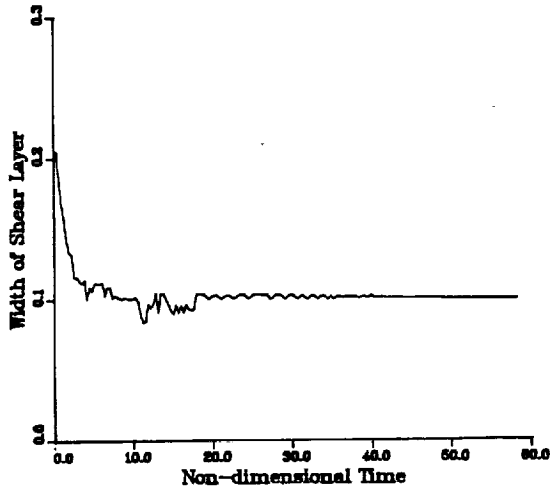

Fig. 12 (a) Width of shear layer with time at leading-edge in natural flow

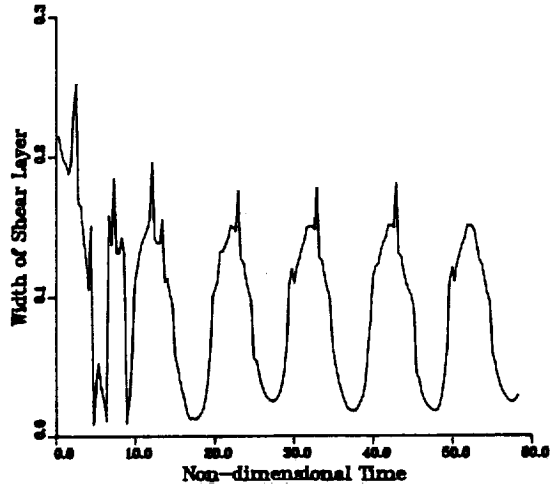

Fig. 12 (b) Width of shear layer with time at leading-edge in excited flow

Fig.12 represents the width of shear at separation as a function of time. Approximately, this width may be regarded as a distance between the core vortex and the wall of body. In non-pulsating flow, as time advances, this width becomes constant. However, in perturbed flow, at St_{max}, it oscillates with the period of $10Ht/U_i$, which corresponds to the forcing frequency St_{max}≈0.1. In perturbed flow, the nascent vortices interact with the surface from the start of the rolling-up motion, so this is related to the resultant amplification of disturbances.

The power spectra, which as defined as eqn.(13), was obtained at the edge of the shear layer where u'/U_i=0.02 and is shown in Fig.13. As pointed out previously, the power spectra of u near reattachment region also discloses the broad peak value around St=0.1. Thus, this

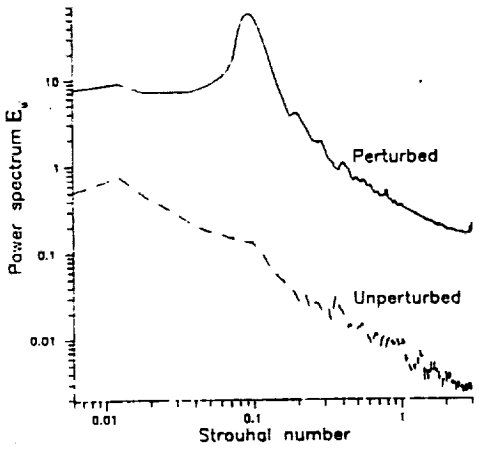

Fig. 13 (a) Power spectrum of u' (=$E_{u'}$) near separation line at the edge of the shear layer (r.m.s. u/U_i≈0.02)

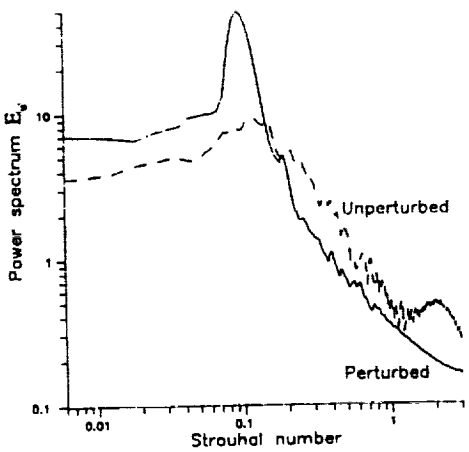

Fig. 13 (b) Power spectrum of u' (=$E_{u'}$) near reattachment position at the edge of the shear layer (r.m.s. u/U_i≈0.02)

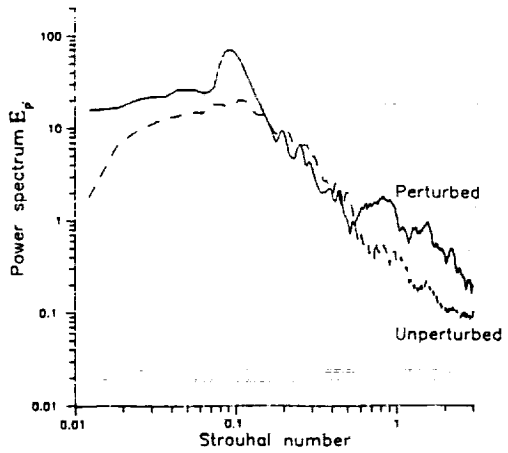

Fig. 14 Power spectrum of p' (=$E_{p'}$) near reattachment position at the edge of the shear layer (r.m.s. u/U_i≈0.02)

frequency(St=0.1) can be considered as the most amplified shedding frequency of large-scale vortices, which is also verified from the power spectra of pressure at the same position(Fig.14).

$$\int_0^{\infty}(E_{u'},E_{p'})\,d(fH/U_i)=\left(\bar{u'}^2/U_i^2\,,\ \bar{p'}^2/\frac{1}{2}\rho U_i^2\right) \qquad (13)$$

In passing, it is notable that the present result tends to have appreciably the same value as the results of Mabey[15]. It gives the relation of $St\cdot X_r$≈0.7 with almost the same value of the present result. This trend has also been noticed in other experimental results[2,3]. It is stressed here that the most amplified shedding frequency gives strong effects on the reduction of reattachment length, drag and enhancement of vortex coalescence in the separation bubble.

The power spectra near separation line shows the broad peak at relatively low frequency(Fig.13(a)). This is regarded as an evidence of the flapping motion of separation bubble, which seems to be attributed to unsteadiness[1,5,16]. Near reattachment region, the low-frequency peak is gradually diminished and the broad peak is centered upon around St_{shed}≈0.1. Roshko[3] called this frequency as the shedding-type instability, which is the dominant frequency in separation bubble.

In this study, we assumed that St_{shed} is identical to St_{max}. This is attributed to the analogy as follows; If the pulsating frequency is higher than the initial Kelvin-Helmholtz frequency St_{KH}, there is no instability region. In this sense, the slow disturbance can not be amplified. Thus St_{shed} becomes dominant around the value of St_{max}.

The way to estimate St_{shed} has been tried through a lot

of experiments. Roshko[3] obtained the relation $fh/U_s \approx 0.08$, where h is the asymptotic height, U_s is the velocity at separation line and f is the shedding frequency corresponding to St_{shed}. In the present case, we obtained the value of $fh/U_s \approx 0.078$, which is nearly identical to that of Roshko. U_s can be obtained from the two-dimensional Bernoulli's equation.

$$\frac{U_s}{U_i} = (1 - C_{ps})^{1/2} \tag{14}$$

It should be noted that the flow geometry of Roshko is different from the present experimental configuration, however, the result gives nearly same trends. Roshko's result was obtained from the frequency of von Karman vortex sheet in a blunt circular cylinder. Levi[17] also suggested the Strouhal Law, which defined as $fd/U_i \approx 0.16$. In this case, if d=2h substituted, his law gives the exactly same value of our result. From the aforementioned comparison, the tentative summary can be suggested that St_{shed} has its origin in the large-scale structures of turbulence, regardless of flow geometries. In this connection, it is believed that St_{max} is approximated by St_{shed}. Thus, this forcing frequency enhances the spreading rate of flow and vortex coalescence and minimizes the drag effectively.

References

[1]Kiya, M., Mochizuki, O., Tanaka, H., and Tsukasaki, T., "Control of a Turbulent Leading-Edge Separation Bubble," Proceedings of IUTAM Sym. on Separated Flow and Jets (Ed. Kozlov, V. V.), Springer-Verlag, 1991.

[2]Roos, F. W. and Kegelman, J. T., "Control of Coherent Structures in Reattaching Laminar and Turbulent Shear Layers," AIAA J., Vol 24, 1986, pp. 1956-1963.

[3]Sigurdson, L. W. and Roshko, A., "The Structure and Control of a Turbulent Reattaching Flow," Turbulent Management and Relaminarization, Springer-Verlag, 1988, pp. 497-514.

[4]Sarpkaya, T. and Itasaka, M., "Inviscid Model of Two-Dimensional Vortex-Shedding by a Circular Cylinder," AIAA J., Vol 17, 1979, pp. 1193-1200.

[5]Kiya, M., Sasaki, K., and Arie, M., "Discrete-Vortex Simulation of a Turbulent Separation Bubble," J. Fluid Mech., Vol 120, 1982, pp. 219-244.

[6]Aso, S., Hayashi, M., Futatsudera, N., and Fujimoto, A., "Numerical Simulation of Separated Flows around a Wing Section by Discrete Vortex Method," Proceedings of International Sym. on CFD at Nagoya, 1989.

[7]Clements, R. R., "An Inviscid Model of Two-Dimensional Vortex Shedding," J. Fluid Mech., Vol 57, 1973, pp. 321-336.

[8]Evans, R. A. and Bloor, M. I. G., "The Starting Mechanism of Wave-Induced Flow through a Sharp-Edged Orifice," J. Fluid Mech., Vol 82, 1977, pp. 115-128.

[9]Chorin, A. J.,"Numerical Study of Slightly Viscous Flow",J. Fluid Mech., Vol 57, 1973, pp. 758-796.

[10]Koenig, K., "Interference Effects on the Drag of Blunt Bodies in Tandem," Ph. D. Thesis, California Institute of Technology, 1978.

[11]Hiller, R. and Cherry, N. J., "Pressure Fluctuations under a Turbulent Shear Layer," 3rd Turbulent Shear Flow Symposium, Davis, California, 1981.

[12]Bhattacharjee, S., Scheelke, B., and Troutt, T. R., "Modification of Vortex Interactions in a Reattaching Separated Flow," AIAA J., Vol 24, 1986, pp. 623-629.

[13]Hussain, A. K. M. F., "Coherent Structure - Reality and Myth," Phys. Fluids, Vol 26, 1983, pp. 2840-2842.

[14]Kiya, M. and Sasaki, K., "Structure of a Turbulent Separation Bubble," J. Fluid Mech., Vol 137, 1983, pp. 83-113.

[15]Mabey, D. G., "Analysis and Correlation of Data on Pressure Fluctuations in Separated Flow," J. Aircraft, Vol 9, 1972, pp. 642-645.

[16]Eaton, J. K. and Johnston, J. P., "Low Frequency Unsteadiness of a Reattaching Turbulent Shear Layer," Turbulent Shear Flows III (Ed. Bradbury, L. J. S., Durst, F., Launder, B. E., Schmidt, F. W., and Whitelaw, J. H.), Springer-Verlag, 1982, pp. 162-170.

[17]Levi, E., "Universal Strouhal Law," ASCE J. Engineering Mech., Vol 109, 1983, pp. 718-727.